F. HIGH PRECISION AND HIGH SENSITIVITY
MEASUREMENTS AND INVESTIGATIONS

The nucleus continues to be one of nature's classic laboratories for investigating both the strong and weak interactions. The equipment and techniques developed for investigating nuclei can be used to tackle many problems in nature. A range of ultra-sensitive investigations was pursued. One area of investigation concerns to fusion mechanism of heavy-ions, especially at very low energies. Beyond these projects, synchrotron radiation from the Argonne Advanced Photon Source (APS) was used to determine the probability in enhancing the decay rate of the 31-year nuclear isomer in ^{178}Hf and refuting earlier claims of substantial enhancements. Investigations into the dynamics of confined plasmas also continued, focusing on the melting of confined cold plasmas. We continue to be interested in finding new avenues where our knowledge and equipment allow us to make significant contributions to important fundamental projects.

f.1.   Measuring the ^{3}He Content of Ultra-Pure ^{4}He: A Step Toward Determining the Neutron's Half-Life to High Precision (R. C. Pardo, K. E. Rehm, R. V. F. Janssens, C. L. Jiang, J. P. Schiffer, R. H. Scott, S. Sinha, R. Vondrasek, D. P. Moehs,* C. Bavlsik,† P. Huffman,‡ J. Doyle,§ S. Dzhosyuk,§ D. McKinsey,§ and L. Yang§)

An experiment to determine the fractional concentration of ^{3}He remaining in isotopically purified ^{4}He was initiated at ATLAS using the technique of Accelerator Mass Spectroscopy(AMS). This measurement is in support of a program to improve the accuracy of the neutron beta-decay lifetime to 1 part in 10^5.

The major difficulty in making this measurement is reducing the helium background coming from materials used in the ion source and achieving stable, high-pressure operation of the source. Last year we reported progress on this project including the design and testing of a new, small quartz MINIECR ion source which significantly reduced the helium background compared to the normal ATLAS ECR ion sources. This year that source design was improved by redesigning the quartz cylinder to remove one uncooled o-ring which limited RF power and made it impossible to run the source with nitrogen or oxygen support gas. This new source design was successfully used in the most recent runs.

In January, 2003 a run with this new source design allowed us to clearly measure the ^{3}He content in highly purified samples used in the neutron lifetime experiment. A variety of source operating modes were compared – helium only, helium + nitrogen feed, and helium + oxygen feed. This combination of source operating conditions made it possible to cleanly measure the residual helium background and clearly demonstrate measurement of the ^{3}He/^{4}He ratio. The data obtained during that run is summarized in Figure I-58.

The value of the ^{3}He/^{4}He ratio measured in this run is $2.6 \times 10^{-13} \pm 1.1 \times 10^{-13}$. Continued work to improve the repeatability of the results is planned. We have some concern as to whether aluminum in our MINIECR is the optimum material for this application and improved measurement of the absolute transmission of ^{3}He in the system is necessary to improve our precision.

_____

*Fermi National Laboratory, †University of Chicago, ‡National Institute of Standards and Technology, §Harvard University.
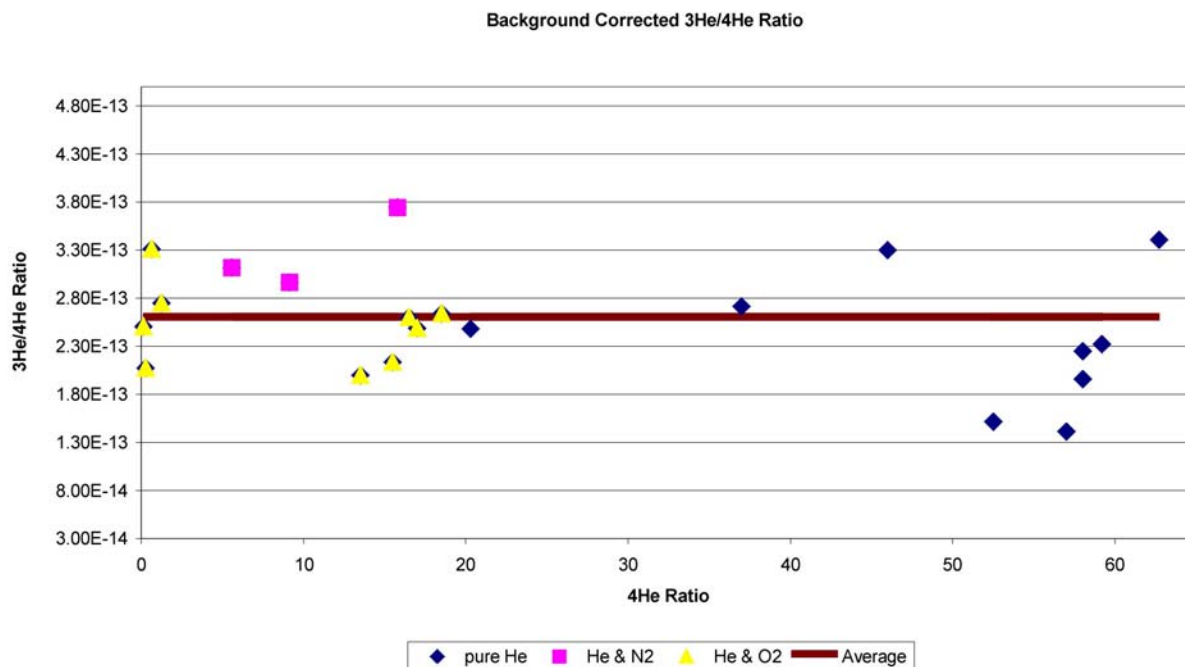
Background Corrected 3He/4He Ratio

Fig. I-58. Background corrected $^3He/^4He$ ratio as a function of ^4He current. A power law curve is shown in green and a linear fit is shown in red. The raw average of all data is $^3He/^4He = 2.6 \times 10^{-13}$.

f.2.   Accelerator Mass Spectrometry of the Heaviest Long-Lived Radionuclides
(I. Ahmad, C. Vockenhuber,* R. Golser,* W. Kutschera,* V. Liechtenstein,†
A. Priller,* P. Steier,* and S. Winkler*)

One of the best ways to determine very low concentrations of long-lived radionuclides is by Accelerator Mass Spectrometry (AMS). The Vienna Environmental Research Accelerator (VERA), based on a 3-MV Pelletron tandem accelerator, was used to measure long-lived radioisotopes at natural abundances across the nuclear chart from ^{10}Be to ^{244}Pu. The facility was recently upgraded to measure heavy ions, which

enabled us to measure isotopes of ^{182}Hf, ^{236}U and ^{244}Pu. The nuclides ^{182}Hf ($t_{1/2} \sim 9$ Ma) and ^{244}Pu ($t_{1/2} = 81$ Ma) are of interest because they are produced in supernovae and may be detectable in deep-sea sediments, which would indicate the occurrence of recent supernovae in relatively close neighborhood to our earth. The results of this methodological AMS study were published.[1]

_____
*University of Vienna, Austria, †Kurchatov Institute, Moscow, Russia.
[1]Int. J. Mass Spectrom. **223-224**, 713 (2003).

f.3.   Precision Measurement of the ^{62}Ga Beta-Decay (G. Savard, D. J. Henderson,
B. Blank,* A. Blazhev,‡ G. Canchel,† M. Chartier,§ J. Döring,‡ Z. Janas,¶
R. Kirchner,‡ I. Muhka,‡ E. Roeckl,‡ and K. Schmidt‡)

As part of the program to extend the set of high-precision superallowed Fermi emitters to heavier systems, we performed a remeasurement of the half-life of ^{62}Ga and a precise branching ratio measurement in this decay. Both measurements were performed at the isotope separator at GSI under experiment number

U192 (spokesperson G. Savard). These measurements will then be completed by the Q-value measurement required to determine the ft-value and together with calculated corrections provide the heaviest point for which a full high-precision data set is available to improve the CVC and CKM unitarity tests.

The data taking for the half-life measurement took place in December 2001. An accuracy of about 0.05% is required for this lifetime. About 20 million β's from the decay of ^{62}Ga were observed with a dedicated 4π gas counter. Over 150000 accumulation and decay cycles were collected with the decay in each cycle observed for about 14 half-lives to properly identify background and contaminant activities. The data were recorded simultaneously with two independent electronics chains of fixed deadtime of 3 and 5 μs respectively. The two data sets can be analysed independently to check for rate dependent systematic errors. Proper software to analyse such data with the required accuracy was developed at Chalk River for a CDC parallel computer. The code corrects for deadtime, removes spectra with detector noise, provides proper statistical weighing of the data point and performs the maximum likelihood fit while also generating simulated spectra to verify that the analysis is performed properly. The code however utilized a number of statistical subroutines proper to the CDC parallel architecture that are not supported by machines now available. It was therefore updated and ported to the SUN cluster where the analysis is being performed. The graphics program GD from GSI was also installed on the SUN cluster and used to provide an easier interface to the output of the analysis program.

Analysis of the data is progressing together with a careful search for possible sources of systematic errors. The analysis for both deadtime settings is in excellent agreement. The data were separated in 39 runs taken with different settings for the detector bias and electronics thresholds. The preliminary results for the individual runs are shown in Fig. I-59. No statistically significant indication of shifts related to these different settings was observed. The data taking also included a γ-ray detector located behind one of the halves of the gas counter and used to look for possible contamination of the mass separated samples. Beta-delayed gammas from the long-lived isotope ^{62}Zn, daughter of the ^{62}Ga decay, are observed but no other contaminant seems to be present. These bounds will be used to determine possible effect of long-lived activity on the measured lifetime. A preliminary value of 116.18(3) ms (statistical error only) is obtained from the analysis at this point. The half-life value seems quite sturdy but the final error bar might change as the analysis progresses.

As a continuation of this work, a measurement of the branching ratio in the decay of ^{62}Ga was also performed this year to help complete the required data set. The measurement was performed in September 2002 with separated samples collected at the GSI on-line isotope separator. Five large γ-detectors, a cluster detector (7 crystals), 2 GSI clovers (each with 4 crystals) and two single crystal detectors, with a total of 17 Ge crystals were used for this experiment. Four silicon detectors were also installed around the collection point to detect the βs. A tape transport system was used to remove long-lived activity. This detector combination will yield β-γ, γ-γ and β-γ-γ data of sufficient quality to determine allowed branches to low lying 1^+ states and non-analog branches to low-lying 0^+ states of sufficient intensity.

The branching ratio data set contains 225 runs for a total of roughly 45 GB of unpacked data. A program to unpack the data in a format acceptable by the DAPHNE analysis program is being modified. The final measurement required, that of the Q-value, is in preparation at the CPT spectrometer.

_____

*Argonne National Laboratory and Centre d'études Nucléaires de Bordeaux-Gradignan, France, †Centre d'études Nucléaires de Bordeaux-Gradignan, France, ‡Gesellschaft für Schwerionenforschung mbH, Darmstadt, Germany, §University of Liverpool, United Kingdom, ¶Warsaw University, Krakow, Poland.
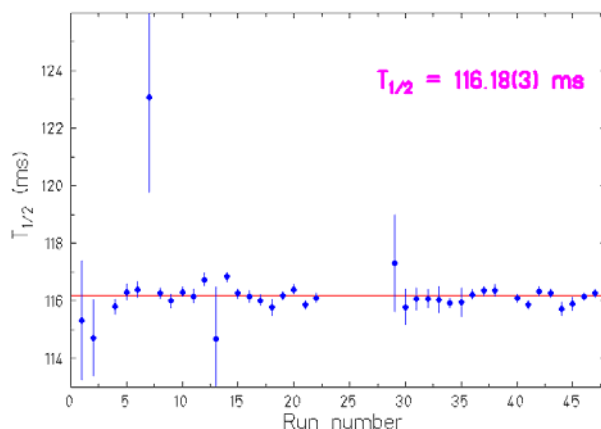
Fig. I-59. Preliminary ^{62}Ga half-life result and variation amongst the 39 runs performed.

f.4.   Search for X-Ray Induced Decay of the 31-yr Isomer of ^{178}Hf at Low X-Ray Energies (I. Ahmad, D. S. Gemmell, E. F. Moore, J. P. Schiffer, J. Banar,* J. A. Becker,† T. A. Bredeweg,* J. R. Cooper,† A. Mashayekhi,‡ D. McNabb,† P. Palmer,* S. Rundberg,* S. D. Shastri,‡ T. F. Wang,† and J. B. Wilhelmy*)

The 31-yr isomer of ^{178}Hf, which has J^{π}, K = 16$^+$,16 and an excitation energy of 2.446 MeV, was the object of several studies for possible mechanisms that might trigger its decay. The potential to control nuclear energies (MeV) with atomic energies (keV) is the driving interest. This isomer is the favorite for this purpose because it is long-lived, available in microgram quantities, has a well known decay scheme, has high excitation energy, and targets can be readily fabricated. The accelerated emission of gamma rays from the ^{178}Hf isomer when irradiated with photons from a dental x-ray machine was first reported by Collins *et al.*[1] The triggering x-ray energy was reported to be in the 20-60 keV range. Using the synchrotron radiation at the Advanced Photon Source (APS) we had published[2] limits on such accelerated emission some 5 orders of magnitude lower than those in Ref. 1. Very recently, a new measurement using monochromatic x rays from the SPring-8 synchrotron was reported by Collins *et al.*[3] They report enhancement in the decay of this Hf isomer for x-ray energies of 9-13 keV. In order to check this observation, we modified our original experiment to extend our sensitivity to lower energy x-rays.

We used a Hf isomeric target that was much thinner than in the previous experiment. It was electroplated onto a Be disk, and the activity was covered by another similar Be disk. This target was then irradiated by the white beam from a tapered undulator at the SRI-CAT 1-ID beam line of the APS. The photon beam was collimated to 1.4×2 mm^2, and the target was placed at 45° with respect to the incident beam. The gamma spectrum from the decay of the isomer was measured with a Ge detector placed at 90° through a set of Pb, Ta, Cd, Cu absorbers. On the other side of the chamber a Si(Li) detector was placed at 90° and at a distance of about 50 cm, with a collimator of .05 × .05-mm^2 in order to reduce the counting rate to a manageable level. This latter detector measured the Hf fluorescent K x-rays during the irradiation to determine the beam luminosity. The beam was cycled as previously: 11 s on-target followed by two 11-s counting periods with the beam-off target. We analyzed the data in all these periods in a way similar to Ref. 2. No significant enhancement was found. Using the upper limit in the difference of gamma-ray peak areas, we calculated the energy-integrated cross sections. These are shown in Fig. I-60 and are several orders of magnitude below the reported values. The results of this investigation were accepted for publication.[4]

_____

*Los Alamos National Laboratory, †Lawrence Livermore National Laboratory, ‡Advance Photon Source, Argonne National Laboratory.
[1]Phys. Rev. Lett. **82**, 695 (1999).
[2]Phys. Rev. Lett. **87**, 072503 (2001).
[3]Europys. Lett. **57**, 677 (2002).
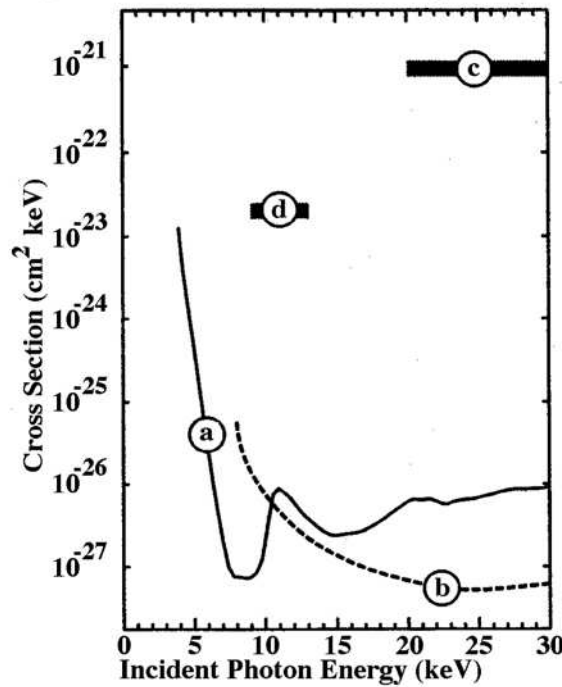[4]I. Ahmad et al., Phys. Rev. C**67**, 041305(R)/1-4 (2003).

Fig. I-60. The upper limit of the integrated cross section for the photon induced de-excitation of the 31-y ^{178}Hf isomer for incident photon energies between 4 and 30 keV from the present measurement is shown as solid line (a). The previous limit from Ref. 2 is shown as dashed line (b). The cross sections from Refs. 1 and 3 are shown as cross-hatched bars (c) and (d).

f.5.   The Fusion Excitation Function for the System ^{64}Ni + ^{64}Ni at Extremely Sub-Barrier Energies (C. L. Jiang, K. E. Rehm, H. Esbensen, R. V. F. Janssens, B. B. Back, C. N. Davids, J. P. Greene, A. M. Heinz, D. J. Henderson, G. Mukherjee, T. Pennington, R. C. Pardo, D. Seweryniak, S. Sinha, M. Paul,* and P. Collon†)

In the simplest picture, fusion reactions between two heavy ions at low energies are governed by the penetration through the interaction barrier (formed by the repulsive Coulomb and the attractive nuclear potentials) followed by absorption inside the barrier. With the discovery of sub-barrier fusion enhancement, it was found that coupling between fusion and other degrees of freedom creates a multi-dimensional potential barrier resulting in increased fusion probabilities. The study of the interplay between the interaction barrier, the tunneling process and the absorption has been restricted mostly to the region in the vicinity of the barrier, for heavy-ion reactions because of difficulties with measuring fusion cross sections below ~100 μb. Naively, one expects that coupled-channels effects should saturate at low bombarding energies and the product σE should therefore exhibit a simple exponential fall-off with decreasing energy.[1]

Measurements of fusion reactions between heavy-ions at extreme sub-barrier energies is of interesting for reaction mechanism studies as well as for their astrophysical consequences. It was pointed out recently[2] that, at these energies, the fusion cross sections exhibit a behavior that is different from the predictions of coupled-channels calculations, with a much steeper falloff observed at energies far below the Coulomb barrier for the systems ^{58}Ni + ^{58}Ni,[3] ^{90}Zr + ^{90}Zr, ^{92}Zr and ^{89}Y,[4] and ^{60}Ni + ^{89}Y.[2] This feature is emphasized in the so-called logarithmic derivative, $L(E) = d(ln(\sigma E))/dE$, which continues to increase with decreasing energies.

Recently, we measured fusion-evaporation cross sections in the system ^{64}Ni + ^{64}Ni. This system was selected because 1) it was studied previously by two groups (Beckerman *et al.*[5] and Ackermann *et al.*[6]), and it was compared with coupled-channels

calculations; 2) to avoid complications arising from reactions on small amounts of heavier isotopic contaminants in the target, or lower-Z isobaric contaminants in the beam which can dominate the low-energy yields, the ^{64}Ni + ^{64}Ni system is free of these complications.

The experiment was performed at ATLAS with the Fragment Mass Analyzer (FMA). The target used was isotopic ^{64}Ni metal, evaporated on a thin carbon foil (100 μg/cm^2) with a thickness of 82 μg/cm^2. The detection technique for the residues used in the experiment and the data analysis are rather similar to our previous experiment.[2] Due to the installation of a split anode in the first electric dipole of the FMA, the background from scattered beam particles was greatly reduced.

The fusion-evaporation cross sections were measured down to the 100 nb region. The results are shown in Fig. I-61, together with the cross sections obtained in Refs. 5 and 6, respectively. At the lowest energy, no events have been observed. The upper limit in Fig. I-61 represents the cross section for one count. Our measurements are in good agreement with the results from Ref. 5, but are shifted by about 2 MeV (in the laboratory system) towards lower energies, compared to

the results from Ref. 6. Such a shift was observed similarly earlier for the system ^{64}Ni + ^{92}Zr measured at ANL[7] and at Legnaro.[8] The systematic energy differences are not important for the discussions of the derivatives. However, we are planning to recalibrate the energy of the ^{64}Ni beam at ATLAS in the near future. Compared to the previous experiment, our results extend the fusion cross sections measurement by about three order of magnitudes.

The logarithmic derivatives $L(E)$ are shown as function of E in Fig. I-62 including results obtained from earlier experiments. For the system ^{64}Ni + ^{64}Ni, the values $L(E)$ extracted from data again show an increase with decreasing energy. The coupled-channels calculation (shown by the dashed curve) is found to increase only modestly at low energies. A similar result is observed for a one-dimensional barrier penetration calculation (see dotted curve). The solid curve, $L_0(E)$ represents an s-wave transmission for a pure Coulomb potential, which is discussed in the subsequent contribution.[9] At the lowest energies, the three curves are nearly parallel but all are unable to describe the general behavior of the experimental results, indicating that a yet to be identified physical contribution is missing in the description of the reaction.

_____

*Hebrew University, Jerusalem, Israel, †Columbia University.
[1]R. Vandenbosch, Annu. Rev. Nuc. Part. Sci. **42**, 447 (1992).
[2]C. L. Jiang *et al*., Phys. Rev. Lett. **89**, 052701 (2002).
[3]M. Beckerman *et al*., Phy. Rev. C **23**, 1581 (1982).
[4]J. G. Keller *et al*., Nucl. Phys. **A452**, 173 (1986).
[5]M. Beckerman *et al*., Phys. Rev. C **25**, 837 (1992).
[6]D. Ackermann *et al*., Nucl. Phys. **A609**, 91 (1996).
[7]W. Henning *et al*., private communications (1993).
[8]A. M. Stefanini *et al*., Phys. Lett. **B252**, 43 (1990).
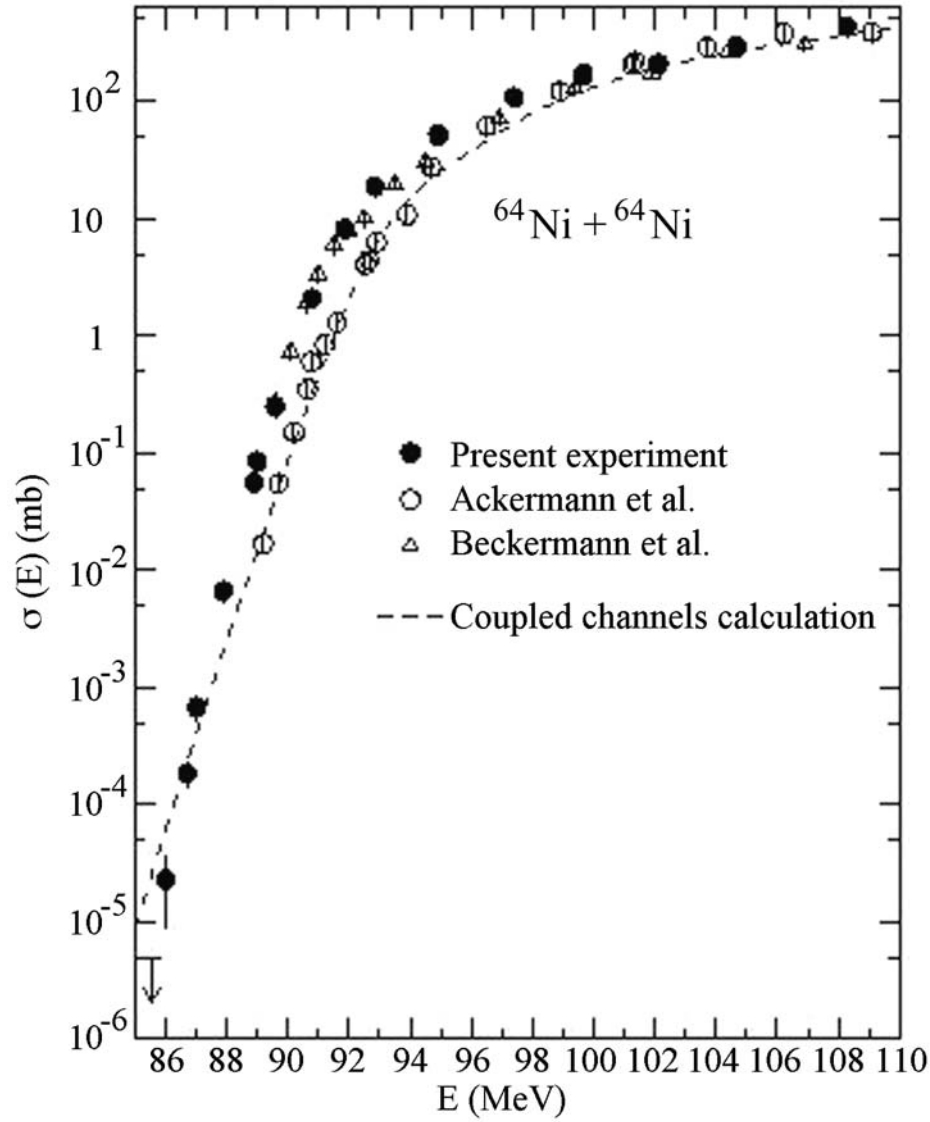[9]C. L. Jiang *et al*., see annual report f.6.

Fig. I-61. Experimental evaporation residue cross sections σ(E) plotted as function of the center-of-mass energy E
for the system ⁶⁴Ni + ⁶⁴Ni. The incident energies have been corrected for the finite target thickness (including the
effect of sharp changes in the excitation function with energy). The uncertainties in the cross sections for many
points are smaller than the size of the symbol. The dashed curve shows the coupled-channels calculations fitted to
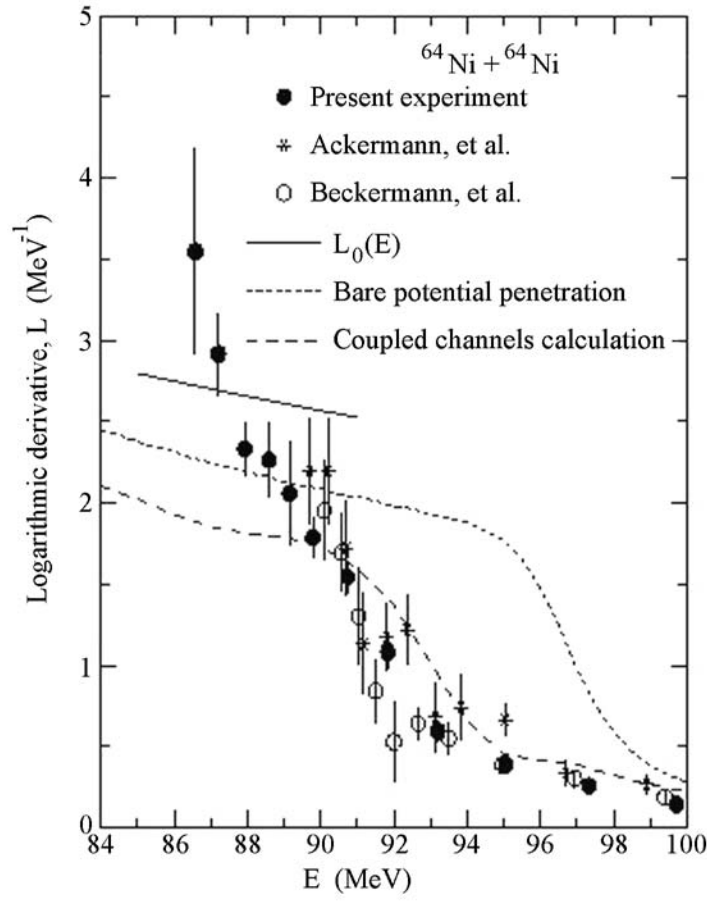*the results of Ref. 6.*

Fig. I-62. Logarithmic derivative L(E) = d(ln(σE))/dE, plotted as function of center-of-mass energy E for the systems $^{64}Ni + ^{64}Ni$, obtained from least-squares fits to three neighboring cross sections points. Dashed line and dotted lines are the results of theoretical calculations using the coupled-channels formalism or a one-dimensional barrier penetration without coupling, respectively. The solid line is obtained from an s-wave transmission as discussed in the subsequent contribution.

f.6.   The Behavior of Heavy-Ion Fusion Reactions at Extreme Sub-Barrier Energies
(C. L. Jiang, H. Esbensen, K. E. Rehm, B. B. Back, and R. V. F. Janssens)

The asymptotic behavior of reaction cross sections at extremely low energies is very important for calculating reaction rates in nuclear astrophysics. To compensate for the rapid energy dependence at very low energies, the so-called S-factor has been introduced, which is defined by the equation:

$$\sigma E = S(E)e^{-2\pi\eta}. \qquad (1)$$

Here, E is the center-of-mass energy and η is the Sommerfeld parameter. This parameterization is based on the pure s-wave scattering in a Coulomb potential between point like nuclei. In light-ion reactions (e.g. (p,γ)), the data usually exhibit a constant S-factor[1] if extrapolated towards very low energies. This parameterization has also been used for light-heavy-ion reactions, (e.g. $^{12}C + {}^{16}O^{2}$ and $^{16}O + {}^{16}O$ etc.[3-5]),

although the fusion reactions for these systems are not restricted to s-wave scattering even at rather low energies. For these cases the S-factor is found to be flat or only weakly dependent on the energy as well, in the vicinity of the lowest energies.

When using the parameterization of Eq. (1) for fusion reactions induced by medium-mass nuclei, an interesting and unexpected result is observed. In Fig. I-63, the S-factor is plotted for five medium-mass systems, which were studied to low enough energies ($^{58}Ni + {}^{58}Ni,[6] {}^{90}Zr + {}^{92}Zr$ and $^{89}Y,[7] {}^{60}Ni + {}^{89}Y[8]$ and $^{64}Ni + {}^{64}Ni[9-11]$). In all these systems one observes a maximum in $S(E)$ followed by a steep decrease at the lowest energies. Extending these studies towards even lower energies is very difficult, since the cross sections mostly are already in the sub-μb region.
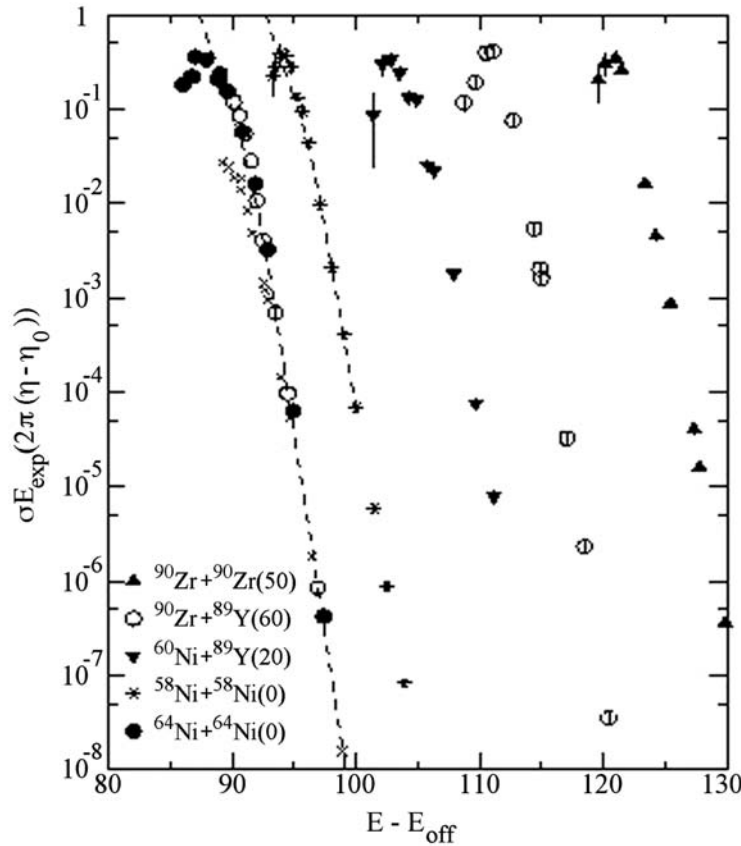

Fig. I-63. Plots S(E) vs. E - E_{off} for the systems $^{64}Ni + {}^{64}Ni$, $^{58}Ni + {}^{58}Ni$, $^{60}Ni + {}^{89}Y$, $^{90}Zr + {}^{89}Y$ and $^{90}Zr + {}^{92}Zr$. The E_{off} values are 0, 0, 20, 60 and 50 MeV, respectively. Dashed curves are the results of coupled-channels calculations.

The phenomenon observed here is closely related with the observation,[8,11] that the fusion cross sections exhibit a behavior which is different from the predictions of coupled-channels calculations, with a much steeper falloff at energies far below the Coulomb barrier. To discuss this effect, the logarithmic derivative, $L(E) = d(ln(\sigma E))/dE$, has been introduced.

In order to understand these two phenomena and the difference in the behavior for light and medium (and heavy) mass systems, we consider the fusion cross section formula

$$\sigma_{fusion}(E) = \frac{\pi}{k^2} \sum_{l=0}^{\infty} (2l+1)P_l(E)A_l. \quad (2)$$

In Eq. (2) k is the wave vector, $P_l(E)$ is the transmission coefficient for the partial wave l, and A_l is the absorption coefficient. In most cases it is assumed that $A_l = 1$, since the excitation energy and the level density in the compound nucleus are high. This still holds for fusion reactions at $E = 0$, as long as the reaction Q-value is sufficiently positive. Under these conditions, one obtains a finite (although extremely small) cross section at very low energies. Using Eq. (1), one finds that at $E = 0$, both the product σE as well as the factor $exp(-2\pi\eta)$ approach zero, but not $S(E)$, which can remain at a finite value. All light-ion induced reactions studied so far, which are of astrophysical interest, have positive Q-values and, thus, finite S-factors are observed.

The situation changes for fusion reactions induced by medium or heavy mass nuclei. In these cases the Q-values are mostly negative (for the five systems in Fig. I-63, Q-values range from -48.783 to -157.35 MeV). For a negative Q-value, the fusion cross section must be zero below $E = -Q$, because of energy conservation. Since no compound nucleus formation is possible under these conditions, fusion cross section must be zero. Since at $E = -Q$, the factor $exp(-2\pi\eta)$ is finite, one needs to have $S(E) = 0$ at $E = -Q$ in order to fulfill Eq. (1). Thus, one expects, that the $S(E)$ factor should exhibit a maximum for all systems with negative Q-values as shown in Fig. I-63.

For medium and heavy-mass system, at energies where $E \ll E_c$ (Ec is the Coulomb barrier), or equivalently, when the classical turning point is much larger than the nuclear radius, the transmission for an s-wave (point charge approximation) is:[12]

$$P_0 = 2\pi\eta \frac{1}{exp(2\pi\eta) - 1} \approx 2\pi\eta\, exp(-2\pi\eta), \quad (3)$$

and the corresponding logarithmic derivative is

$$L_0(E) = \frac{dln((\sigma E)_0)}{dE} \approx \frac{\pi\eta}{E}, \quad (4)$$

where the Sommerfeld parameter is typically larger than 50.

---
[1]C. E. Rolf and W. S. Rodney, Cauldrons in the Cosmos, The University of Chicago press (1988).
[2]B. Cujec *et al.*, Nucl. Phys. **A266**, 461 (1976).
[3]R. G. Stokstad *et al.*, Phys. Rev. Lett. **37**, 888 (1976).
[4]H. Reeves, Ap. J. **135**, 779 (1962).
[5]S. Schramm and S. E. Koonin *et al.*, Ap. J. **127**, 296 (1990).
[6]M. Beckerman *et al.*, Phy. Rev. C **23**, 1581 (1982).
[7]J. G. Keller *et al.*, Nucl. Phys. **A452**, 173 (1986).
[8]C. L. Jiang *et al.*, Phys. Rev. Lett. **89**, 052701 (2002).
[9]M. Backerman *et al.*, Phys. Rev. C **25**, 837 (1992).
[10]D. Ackermann *et al.*, Nucl. Phys. **A609**, 91 (1996).
[11]C. L. Jiang *et al.*, see annual report f.5.
[12]M. Abramowitz, in *Handbook of Mathematical Functions*, eds. M. Abramowitz and I. Stegun, Dover Publications, Inc., New York, 1964.

Calculated results of the function $L_0(E)$ are given in Fig. I-64 by the solid lines for four of the six systems mentioned above.   In the figure, coupled-channels calculations are available for ^{58}Ni + ^{58}Ni and ^{64}Ni + ^{64}Ni, which are shown as dashed curves. $L_0(E)$ may represent an extreme value of $L(E)$, because it implies a s-wave penetration of the Coulomb potential all the way to r = 0 (under the assumption of A_0 = 1). The slope $L(E)$ extracted from the data exceeds the value of $L_0(E)$. This could be a common behavior of all heavy-ion fusion reactions with negative Q-values, as discussed in Ref. 8.

The curves $L(E)$ extracted from the data cross the function $L_0(E)$ at E_s. From Eq. (1-3) it can be shown easily that this occurs exactly at the energy where the $S(E)$ curve shown in Fig. I-63 has a maximum.

It is surprising that these phenomena occur at such high excitation energies of the compound nuclei (17 - 44 MeV for these six systems). This indicates that some approximation made for calculating the transmission or the absorption coefficients may not be correct.
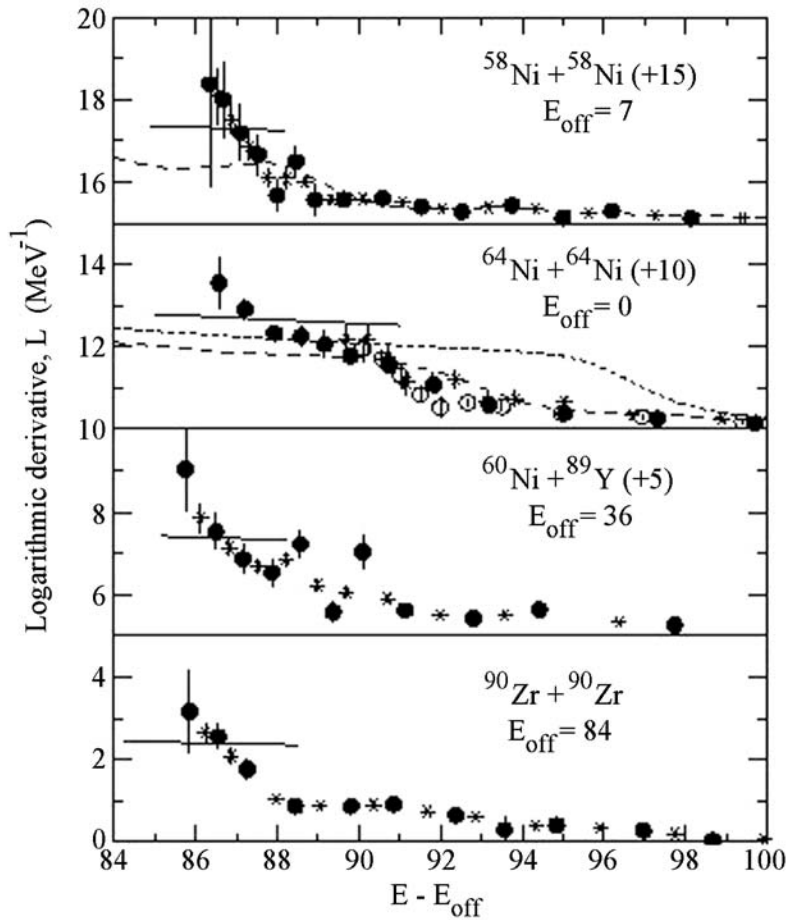

Fig. I-64. Logarithmic derivative L(E) plotted as function of E-E$_{off}$ for systems ^{58}Ni + ^{58}Ni, ^{64}Ni + ^{64}Ni, ^{60}Ni + ^{89}Y and ^{90}Zr + ^{92}Zr. The E$_{off}$ values are 7, 0, 36, 84 MeV, respectively. For ^{64}Ni + ^{64}Ni, the L(E) values are obtained from least-squares fits to three neighboring cross section points. Solid circles, stars and open circles are results from present,[11] Refs. 10 and 9 measurements, respectively. For the other three systems, solid circles and stars correspond to determinations of the logarithmic derivative from consecutive data points and from least-squares fits to three points. Dashed curves are the results of coupled-channels calculations, the dotted curve is an one-dimensional barrier penetration calculation and the solid curve, L$_0$(E) represents an s-wave transmission for a pure Coulomb potential.

f.7. Progress in Measuring the Radiative Capture Cross Sections in ^{12}C + ^{12}C

(C. J. Lister, M. P. Carpenter, S. Freeman, N. Hammond, R. V. F. Janssens, T. L. Khoo, T. Lauritsen, A. H. Wuosmaa, D. G. Jenkins,* B. R. Fulton,* J. Pearson,* P. Fallon,† A. Gorgen,† A. O. Macchiavelli,† M. McMahan,† M. Freer,‡ and F. Haas§)

Radiative capture of heavy ions, their complete fusion without particle evaporation, is an unusual and interesting reaction channel. It may be important in understanding the connection between the numerous resonances in the ^{12}C + ^{12}C fusion and reaction cross sections, and the underlying states in the fused ^{24}Mg compound nucleus. These connections have been sought for many years. The seminal work of Sandorfi and Nathan[1] showed that studying the very high energy gamma-rays from the capture states to levels near the ^{24}Mg groundstate could yield considerable insight into this issue. However, the "1 step" capture decays are only a small part of the radiative capture process. Gamma ray spectroscopy involving the intermediate "doorway" states following radiative capture can provide insight both into the fusion mechanism and into the structure of exotic, highly deformed states in ^{24}Mg.

Earlier experiments using Gammasphere as a calorimeter,[2] picking out radiative capture through its high, positive Q-value, were successful in demonstrating that multi-step gamma decays are very important and that rather few "doorway" states are involved. However, the response of Gammasphere for very high energy gamma rays is not well categorized, so only an estimate of the multi-step radiative capture cross section could be achieved.

To measure the absolute radiative capture cross section for ^{12}C + ^{12}C, we performed a direct measurement of the ^{24}Mg residues using the Argonne Fragment Mass Analyzer (FMA) and an ion chamber. Measuring the fused residue yield directly has different systematic uncertainties than the gamma ray measurements, so serve to confirm the results obtained previously. In addition, selecting the optimum conditions for running the FMA provided a precursor to the final goal of performing a combined Gammasphere-FMA study in the future. The experiment was very successful. ^{24}Mg could be clearly detected in the ion chamber, as evidenced by detecting the 1368-keV first excited state decay at the target position. Considerable attention was paid to producing ^{24}Mg through the competing ^{13}C(^{12}C,n)^{24}Mg and ^{16}O(^{12}C,α)^{24}Mg background contaminant reactions. Several cross-checks were possible to measure the contributions from these undesirable ^{24}Mg ions, and eliminate them from the estimate of radiative cross section. Most importantly, the ^{24}Mg ions associated with fusion have a well defined energy, close to half the beam energy, so can be separated from the ^{24}Mg produced in other reactions by directly measuring their energy in the ion chamber, and through measuring their time of flight. Evaporation and Q-value effects shift the ^{24}Mg ions from the background reactions away from this region. We performed measurements with targets of several thicknesses to look for resonances in yield and seek consistency of measurement. We are performing final analysis of the data to establish a reliable total cross section for radiative capture, but it is clearly ~3 µb, more than a factor of five bigger than the "1-step" decays studied by Sandorfi and Nathan.

We are preparing a manuscript for publication in Physical Review Letters in 2003.

_____

*University of York, United Kingdom, †Lawrence Berkeley National Laboratory, ‡University of Birmingham, United Kingdom, §Centre National de la Recherche Scientifique, Strasbourg, France.

[1]A. M. Sandorfi, "Treatise on Heavy Ion Science", Vol. 2, ed. D. A. Bromley (Plenum 1984) p. 53 and references therein.

[2]D. G. Jenkins. et al., "Frontiers of Nuclear Structure", eds. P. Fallon and R. Clark (American Institute of Physics 2003) p. 329.

f.8.   Elastic Scattering of ^{17}F from ^{208}Pb Near the Coulomb Barrier (K. E. Rehm, J. P. Greene, A. Heinz, D. J. Henderson, C. L. Jiang, E. F. Moore, R. C. Pardo, A. H. Wuosmaa, J. F. Liang,** M. Romoli,* M. Mazzocco,† E. Vardaci,* M. Di Pietro,* R. Bonetti,‖ A. De Francesco,* A. De Rosa,* T. Glodariu,†‡ A. Guglielmetti,‖ G. Inglima,* M. La Commara,* B. Martin,* D. Pierroutsakou,* M. Sandoli,* C. Signorini,† F. Soramel,§ and L. Stroe¶)

Elastic scattering of ^{17}F nuclei from ^{208}Pb was measured at 90.4 MeV incident energy in the angular range θ_{lab} = 98° - 154°. The ^{17}F beam was produced with the In-Flight technique via the inverse p(^{17}O,^{17}F)n reaction. The ^{17}F beam intensity on target was about 10^6 pps. The scattered particles were detected using large-area (50 × 50 mm^2) solid-state detector telescopes with thicknesses of 60 µm (ΔE) and 500 µm (ER), segmented into 100 strips on the front.   For a measurement of the angular distribution, the strips of the ΔE detectors were oriented perpendicular to the beam direction. The strips of the ER detectors were oriented orthogonal to those, allowing a determination of the position of particles passing through the ΔE detector with an accuracy of 0.5 mm. The readout of the position information was obtained using ASIC chips. The data stream from the chip contains, for each

hit, the strip identification number, the TOT (Time Over Threshold) and the Jitter Time (the time distance between the event trigger and the strip signal).   The energy of the ions is obtained with standard electronics using the backside of the detectors which is not segmented.

In the event analysis, the elastically scattered ^{17}F ions were selected from the contaminant ^{17}O beam on the basis of their energy distributions, as shown in Fig. I-65. Both ^{17}F and ^{17}O ions were stopped in the ΔE detectors. Due to the experimental energy resolution, it was not possible to separate the contribution from the first excited state in ^{17}F at 495.3 keV. From DWBA calculations its contribution is estimated to be less than 2%.
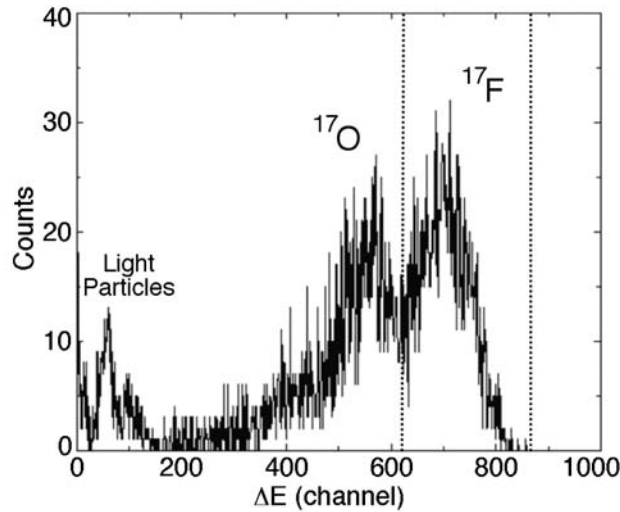

Fig. I-65. Energy spectrum of particles detected by the ΔE layer of the telescope.

Preliminary results from the experiment are shown in Fig. I-66. The solid points represent the experimental data, corrected for the efficiency of the detection apparatus and normalized to the Rutherford cross section. Optical model calculations were performed with the code FRESCO [I. J. Thompson, Comp. Phys. Rep. **7**, 167 (1998)] using a χ^2 minimizing procedure to find the optimum values of the potential. Woods-Saxon shapes for the real and imaginary parts of the potential and different families of the parameters were used (r_0 =

r_W = 1.20, 1.24 fm and a_0 = a_W = 0.43 - 0.73 fm) following the procedure used previously for the ^{19}F + ^{208}Pb system at 91 MeV [C. J. Lin *et al.*, Phys. Rev. C **63**, 064606 (2001)]. From the least-squares fits it is possible to obtain the strong absorption radius (r_{saV} = 11.97 ± 0.14 fm and r_{saW} = 13.50 ± 0.19 fm) and to extract the related potentials: V_{sa} = 3.84 ± 0.51 MeV and W_{sa} = 0.020 ± 0.002 MeV. These values are different from those obtained for the stable system ^{19}F + ^{208}Pb, where the two radii (r_{saV}, r_{saW}) are very similar

(~12.2 fm), while for ^{17}F + ^{208}Pb a difference of about 1 fm is observed. Using the same parameter set ($r_0 = r_W = 1.24$ fm and $a_0 = a_W = 0.53$ fm) for both the systems, the real part of the potential is found to be 30% less deep in the present case, while the imaginary one is

deeper by about 60%. These results give an indication of the sensitivity of elastic scattering measurements to the role played by weakly bound nucleons for a determination of optical model parameters.   The breakup cross sections are presently being analyzed.

∗University and INFN of Napoli, Italy, †University and INFN of Padova, Italy, ‡NIPNE, Bucharest, Romania, Italy, §University and INFN of Udine, Italy, ¶INFN of LNL, Legnaro, Italy, ‖University and INFN of Milano, **Oak Ridge National Laboratory.
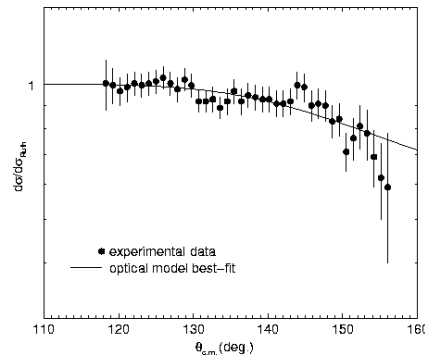

Fig. I-66. Ratio between the elastic scattering cross sections and the Rutherford values in the system $^{17}F + {}^{208}Pb$. The experimental data (circles) are compared to an optical potential model calculation. The parameters used are $r_0 = r_W = 1.24$ fm, $a_0 = a_W = 0.53$ fm, $V = 60.55$ MeV and $W = 5.71$ MeV.

f.9.   Deviations from Constant Density in Confined Plasmas (J. P. Schiffer)

The behavior of a cold plasma cloud that is confined in an external field (such as an ion trap or an accelerator storage ring), was previously studied. Such systems settle into arrays with concentric layers, whose shapes are determined by that of the external confining field. Within each layer the ions arrange themselves in a triangular lattice with equilateral triangles.   The macroscopic density of the cloud is constant, with a sharp outer surface determined by the boundary conditions of the confinement. The interior layers (or shells) are equally spaced and each has the same areal density of ions.

This **constant density** depends on three conditions that have to be fulfilled:

- The ion cloud must be **three-dimensional**.

- The confining field has to be **harmonic** (the restoring force proportional to the displacement from the origin, though the constant of

proportionality can be different in different dimensions).

- The force between the particles has to be a **Coulomb force** (a repulsive force varying as $1/r^2$).

The consequences of deviations from these conditions were investigated by Molecular Dynamics simulations.

Ions Confined To Fewer Than Three Dimensions. Such confinement can occur in the 1-dimensional case, whenever the focusing forces in 2 dimensions are much stronger than the weak *harmonic* force along one axis, for instance in a so-called linear trap pushed to its limits or in a beam bunch in a storage ring.   An example of such a *one-dimensional* configuration is shown in Fig. I-67 along with the spacings between the ions.   It is evident that the density of ions is not uniform: the ions are more densely packed in the interior than near the ends.
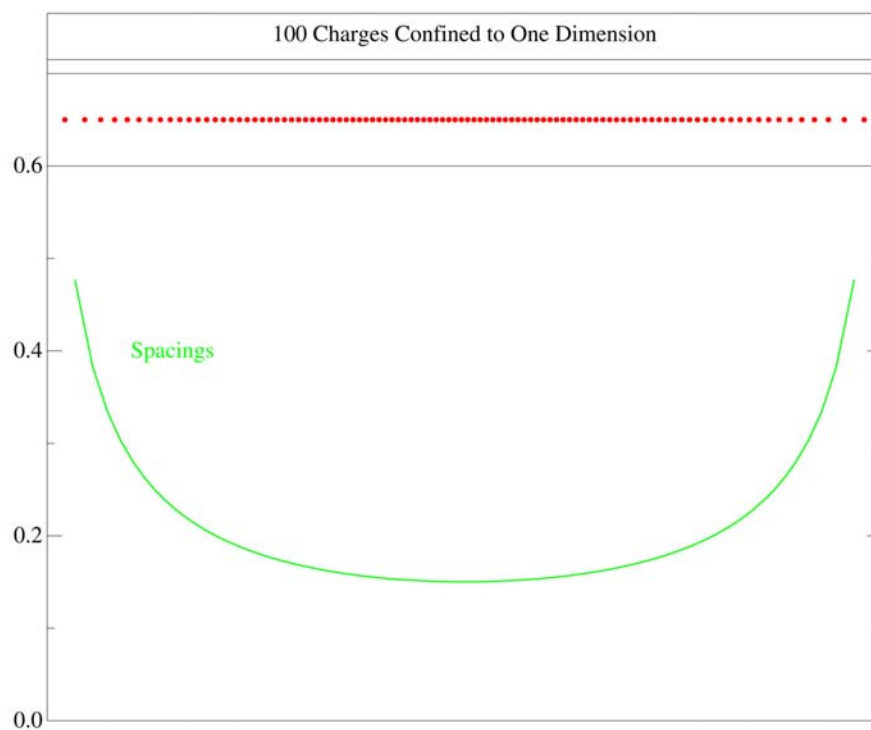
Fig. I-67 One hundred ions on a line confined by a harmonic force.

Similarly, a system of charges on a surface, and then confined within the surface by a harmonic force, is also shown in the lower part of Fig. I-68. Here also it is evident that the density of ions along the periphery of the disk is lower than in the central region.
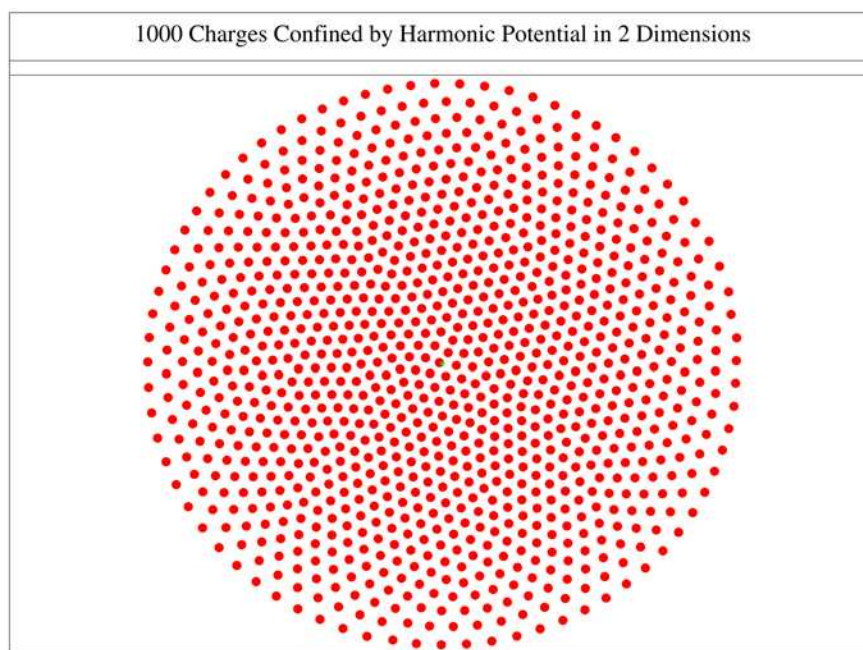

Fig. I-68. One thousand ions confined on a surface by an isotropic harmonic force.

Ions Confined By Non-Harmonic Forces.   Such confinement may be produced in a variety of ways. For instance, rf quadrupole fields (Paul traps) produce an effective potential that corresponds to a harmonic force. But rf traps with more electrodes will produce potentials that will change with a correspondingly higher power of the radius. Another example is in the "linear traps" which have an rf quadrupole field to confine a cloud perpendicular to the long axis, but confinement in the third dimension is usually provided by a biasing electrode with a force that is localized at the ends of the trapping region.   Several cases are considered below, not all of which correspond to specific existing traps.

- *Square-well in three dimensions* implies a force that is infinitely strong at a given radius. The consequence of this is the same as for charges in a conducting sphere.   By Gauss's theorem, since there is no force in the interior, all charges will be on the surface defined by the radius of the square well.

- *Radial dependence **faster** than r^2* can take many forms other than the limiting case of a square well. It can be an exponential potential or one that is a simple higher power of the radius. In Fig. I-69 the case is shown for a potential that is proportional to r^{12}.   It is evident that the (cold) ions are concentrated with increasing density toward the outside and there is a hollow space in the interior with the radius 0.69 times that of the outer sphere. The surface density in the shells increases with radius, approximately as r^9 and the spacing between the shells decreases roughly as $1/r^3$.
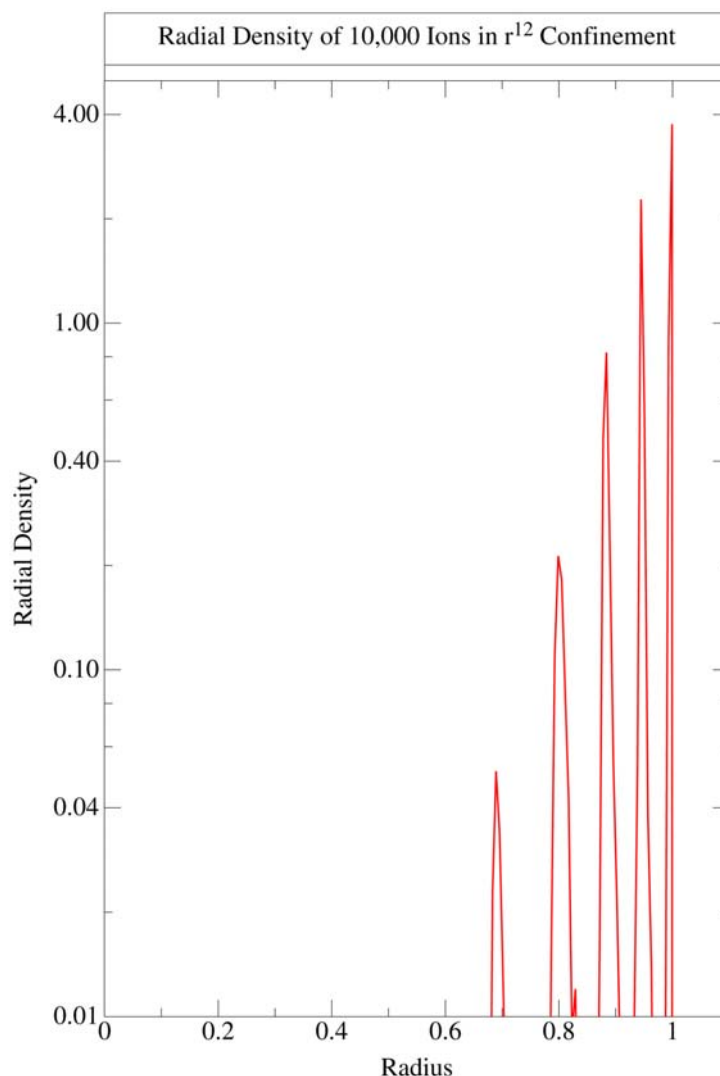

Fig. I-69. *Radial density in a potential that varies as r^{12}.*

- *Radial dependence **slower** than $1/r^2$.* There are many possible functional forms, for the force, from a screened harmonic force: $-K\,r\,e^{-kr}$ to a force that is constant and pointing toward the origin. All of these have in common a density that is increasing toward the center of the cloud, with corresponding changes in the shell structure.

- *Square well in one dimension, harmonic well in others.* This arrangement is an approximation to the confining field in a linear trap. The resulting

configuration is shown in Fig. I-70 where it is seen that the sharp cutoff in density gives rise to a disk of charge, an endplate to the ion cloud. The density of ions on this surface is much higher than the other surfaces. The rest of the ions arrange themselves along roughly cylindrical surfaces in the space in between, with the radius of the endplates larger than that of the cylinders. There is also a tendency for disks parallel to the endplate to appear near the ends.
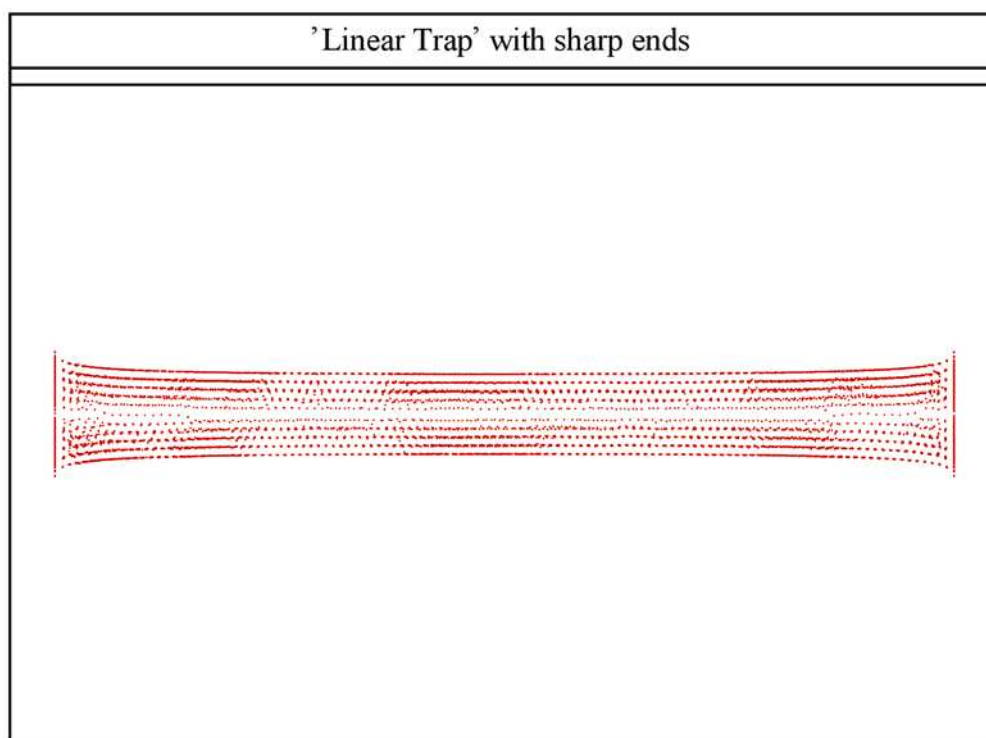
-

Fig. I-70. 10,000 ions confined by a harmonic force in two dimensions and a square well in the third. The projection corresponds to a 180 degree rotation of a plane about the long axis showing the radius vs the z-coordinate of the ions.

- *Square well in two dimensions, harmonic in the third.* This potential would result in a cylinder with high charge density and interior cylinders of lower density.

Interparticle Forces That Are Not Coulombic. Simulations were tried where the interparticle forces are changing *faster* than $1/r^2$, such as a Yukawa-like screened Coulomb force: e^{-kr}/r^2, and this results in densities that are higher in the interior than near the

surface. With forces that are changing more slowly with distance than the Coulomb force the density in the interior is lower than near the surface.

Some values for spherically symmetric confinement are shown in the Table I-4 for the fraction of ions that are in the surface layer and the ratio of ions in the outer third of the volume to those in the inner third.

Table I-4. Effects of various confining potentials and interparticle forces with 10,000 ions.

Radial Confinement	Interparticle Force	Fraction of Ions in Outer Shell	Ratio of Ions in Outer/Inner Thirds of Volume
$-Kr$	$1/r_{ij}^2$	19%	1.000
Square well	$1/r_{ij}^2$	100%	∞
$-Kr^{11}$	$1/r_{ij}^2$	46%	112
$-K$	$1/r_{ij}^2$	15%	0.54
$-Kre^{-kr}$	$1/r_{ij}^2$	15%	0.61
$-Kr$	$1/r_{ij}$	37%	2.9
$-Kr$	e^{-krij}/r_{ij}	11.9%	0.55